Microscopic calculations based on chiral two- and three-nucleon forces for proton- and ^{4}He-nucleus scattering

Masakazu Toyokawa,[1,*] Masanobu Yahiro,[1] Takuma Matsumoto,[1] Kosho Minomo,[2] Kazuyuki Ogata,[2] and Michio Kohno[2]
[1]*Department of Physics, Kyushu University, Fukuoka 812-8581, Japan*
[2]*Research Center for Nuclear Physics (RCNP), Osaka University, Ibaraki 567-0047, Japan*
(Received 10 July 2015; published 25 August 2015)

We investigate the effects of chiral three-nucleon force (3NF) on proton scattering at 65 MeV and ^{4}He scattering at 72 MeV/nucleon from heavier targets, using the standard microscopic framework composed of the Brueckner-Hartree-Fock (BHF) method and the g-matrix folding model. For nuclear matter, the g matrix is evaluated from chiral two-nucleon force (2NF) of N^{3}LO and chiral 3NF of NNLO by using the BHF method. Because the g matrix thus obtained is numerical and nonlocal, an optimum local form is determined from the on-shell and near-on-shell components of g matrix that are important for elastic scattering. For elastic scattering, the optical potentials are calculated by folding the local chiral g matrix with projectile and target densities. This microscopic framework reproduces the experimental data without introducing any adjustable parameter. Chiral-3NF effects are small for proton scattering, but sizable for ^{4}He scattering at middle angles where the data are available. Chiral 3NF, mainly in the 2π-exchange diagram, makes the folding potential less attractive and more absorptive for all the scattering.

DOI: 10.1103/PhysRevC.92.024618 PACS number(s): 21.30.Fe, 24.10.Ht, 25.40.Cm, 25.55.Ci

I. INTRODUCTION

An important current issue in nuclear physics is to understand the effects of three-nucleon force (3NF) on finite nuclei, nuclear reactions, and nuclear matter. Quantitatively decisive roles of 3NFs have been established in properties of light nuclei as well as of nuclear matter [1]. This issue started with the 2π-exchange 3NF proposed by Fujita and Miyazawa [2]. Recently, a major breakthrough was made on this issue with chiral effective field theory (Ch-EFT); see Refs. [3,4] and references therein. Ch-EFT is a theory based on chiral perturbation theory to provide a low-momentum expansion of two-nucleon force (2NF), 3NF, and many-nucleon forces. Using this theory, one can define multinucleon forces systematically. The effects of chiral 3NF were analyzed in many papers; e.g., see Ref. [5] for light nuclei, Refs. [6,7] for *ab initio* nuclear-structure calculations in lighter nuclei, and Refs. [8–12] for nuclear matter. Recently the role of chiral four-nucleon forces was also analyzed for nuclear matter [13]. When the g matrix (the effective nucleon-nucleon interaction in nuclear medium) is calculated from chiral 2NF+3NF with the Brueckner-Hartree-Fock (BHF) method, it well accounts for the empirical properties of symmetric nuclear matter [9]. The g matrix depends on the nuclear-matter density ρ; i.e., $g = g(\rho)$. Chiral-3NF effects become more important as ρ increases.

Another important issue in nuclear physics is microscopic understanding of nucleon-nucleus (NA) and nucleus-nucleus (AA) optical potentials. The optical potentials are essential in describing not only elastic scattering but also inelastic scattering and transfer and breakup reactions. In fact, the optical potentials are essential inputs in distorted-wave Born approximation and continuum discretized coupled-channel method (CDCC) calculations [14].

The g-matrix folding model is a standard method of calculating the optical potential microscopically. Actually, many nuclear reactions have been analyzed with the model. In the model, the potential is obtained by folding $g(\rho)$ with projectile and target densities ($\rho_{\rm P}$ and $\rho_{\rm T}$) for AA scattering and with $\rho_{\rm T}$ for NA scattering; e.g., see Refs. [15–19] for $g(\rho)$ and Refs. [20–22] for the folding procedure. The model is called the single-folding (SF) model for NA scattering and the double-folding (DF) model for AA scattering.

For NA elastic scattering, the SF model based on the Melbourne g matrix [16], constructed from the Bonn-B nucleon-nucleon (NN) interaction [23], well reproduces the experimental data with no adjustable parameter. In the folding procedure, the value of ρ in $g(\rho)$ is assumed to be a value of $\rho_{\rm T}$ at the midpoint $\boldsymbol{r}_{\rm m}$ of interacting two nucleons: $\rho = \rho_{\rm T}(\boldsymbol{r}_{\rm m})$. Target-excitation effects on the elastic scattering are thus well described by the SF model based on the local-density approximation.

We have recently investigated chiral-3NF effects on the description of NA scattering [24] and AA scattering [25], ^{12}C + ^{12}C and ^{16}O + ^{16}O, by modifying the Melbourne g matrix by introducing spin- and isospin-dependent multiplicative factors to simulate the 3NF effects. Results have shown that the 3NF effects are small for NA scattering, because the process is mainly governed by the interaction at low density regions. This reinforces the success of calculations using the Melbourne g matrix without considering 3NFs. On the other hand, sizable effects are found for AA scattering at around 80 MeV/nucleon through the repulsive contribution in the real part and the enhanced absorptive potential. However, these are somewhat exploratory, relying on the Melbourne g matrix. In this paper, we present full chiral g matrices parameterized in a three-range Gaussian form on the basis of nuclear matter g-matrix calculations with the 2NF and 3NF of Ch-EFT, and apply them to the SF and DF models.

*toyokawa@phys.kyushu-u.ac.jp

The g-matrix DF model for AA scattering has a practical problem. In nuclear matter calculations, we have to consider two Fermi spheres and the g matrix should be obtained by solving scattering between a nucleon in a Fermi sphere and a nucleon in another Fermi sphere [26,27], but it is quite difficult in practice. In fact, the g matrix is evaluated by solving nucleon scattering from a single Fermi sphere. For consistency with the nuclear-matter calculation, we assumed $\rho = \rho_{\rm T}(\boldsymbol{r}_{\rm m})$ in $g(\rho)$ and applied this framework to ^{3,4}He scattering from heavier targets in a wide range of incident energies from 30 MeV/nucleon to 180 MeV/nucleon [22,28]. The Melbourne g-matrix DF model with the target-density approximation (TDA) well reproduces the data with no adjustable parameter, particularly for total reaction cross sections $\sigma_{\rm R}$ and forward differential cross sections. The DF-TDA model does not include projectile-excitation effects, but it was confirmed by CDCC calculations that the effects are negligible for ^{3}He scattering. Precisely, the effects are appreciable at incident energies lower than 40 MeV/nucleon, but they enhance $\sigma_{\rm R}$ only by a few percent. It is very likely that projectile-excitation effects are even smaller for ^{4}He scattering, because ^{4}He is less fragile than ^{3}He. The practical problem is thus solved for ^{3,4}He scattering. Therefore, this DF-TDA model is used in this paper.

For heavier projectiles than ^{4}He, it is quite difficult to include all projectile-excitation effects explicitly. For such AA scattering, the frozen-density approximation (FDA), $\rho = \rho_{\rm P}(\boldsymbol{r}_{\rm m}) + \rho_{\rm T}(\boldsymbol{r}_{\rm m})$, is often taken as a value of ρ in $g(\rho)$, although $g(\rho)$ is obtained by solving nucleon scattering on a single Fermi sphere. The DF-FDA model includes projectile-excitation effects approximately. The model based on the Melbourne g matrix well reproduces measured $\sigma_{\rm R}$ for $^{12,14-16}$C [29,30] and Ne and Mg isotopes [21,31]. As an important result, the microscopic analyses conclude that ^{31}Ne and ^{37}Mg are deformed halo nuclei. For ^{3,4}He scattering, however, the DF-TDA model always yields better agreement with the experimental data than the DF-FDA model [22,28].

The g matrix obtained is quite inconvenient in many applications, because it is nonlocal and numerical. The Melbourne group showed that elastic scattering is mainly determined by the on-shell part of $g(\rho)$ [16]. Making a χ^2 fitting to the on-shell and near-on-shell components of the g matrix, the group provided $g(\rho)$ with a local (Yukawa) form to make the folding procedure feasible [16,32,33]. The Melbourne g matrix thus obtained accounts for NN scattering in the limit of $\rho = 0$, and the SF model based on the Melbourne g matrix explains NA scattering systematically with no adjustable parameter, as mentioned above.

In this paper, we consider heavier targets such as ^{40}Ca, ^{58}Ni, and ^{208}Pb to make our discussion clear, because the g matrix is evaluated in nuclear matter and the g-matrix folding model is considered to be more reliable for heavier targets. Taking the Melbourne-group procedure [16,32,33], we provide the chiral g matrix with a three-range Gaussian form for each of the central, spin-orbit, and tensor components, because the Gaussian form is much more convenient than the Yukawa form in many applications whereas the two forms yield the same results for NA and AA scattering. The ranges and the depths of individual components are determined for each energy and density so as to reproduce the on-shell and near-on-shell matrix elements of the original g matrix. For the central part of the g matrix, the present ranges of the three-range Gaussian form are (0.4,0.9,2.5) fm and close to those of Ref. [17]. We call the analytic form "Gaussian chiral g matrix" and the original numerical g matrix "original chiral g matrix," when we need to identify the two. The folding model based on the Gaussian chiral g matrix reproduces the experimental data with no adjustable parameter for the present scattering. Therefore, we can investigate chiral-3NF effects on proton and ^{4}He scattering clearly.

In Sec. II, we recapitulate the BHF method for the symmetric nuclear matter with 2NF + 3NF and the folding model for proton and ^{4}He scattering. In Sec. III, the results of the folding model with the Gaussian chiral g matrix are shown for proton and ^{4}He scattering. Section IV is devoted to a summary.

II. THEORETICAL FRAMEWORK

A. Nuclear-matter calculations for 3NF

We recapitulate the BHF method for the case of 2NF+3NF [9]. The 3NF V_{123} is hard to treat even in infinite matter. We then derive an effective 2NF $V_{12(3)}$ from V_{123} by averaging it over the third nucleon in the Fermi sea. After this approximation, the potential energy is reduced to

$$\frac{1}{2}\sum_{\boldsymbol{k}_1\boldsymbol{k}_2}\langle \boldsymbol{k}_1\boldsymbol{k}_2|V_{12}|\boldsymbol{k}_1\boldsymbol{k}_2\rangle_A + \frac{1}{3!}\sum_{\boldsymbol{k}_1\boldsymbol{k}_2\boldsymbol{k}_3}\langle \boldsymbol{k}_1\boldsymbol{k}_2\boldsymbol{k}_3|V_{123}|\boldsymbol{k}_1\boldsymbol{k}_2\boldsymbol{k}_3\rangle_A = \frac{1}{2}\sum_{\boldsymbol{k}_1\boldsymbol{k}_2}\langle \boldsymbol{k}_1\boldsymbol{k}_2|V_{12}^{\rm eff}|\boldsymbol{k}_1\boldsymbol{k}_2\rangle_A, \quad (1)$$

with the effective 2NF,

$$V_{12}^{\rm eff} = V_{12} + \tfrac{1}{3}V_{12(3)}, \quad (2)$$

where the symbol A means the antisymmetrization and $\boldsymbol{k}_i$ denotes quantum numbers of the ith nucleon; note the factor $1/3$ in front of $V_{12(3)}$ in Eq. (2). The g matrix g_{12} is then obtained by solving the equation,

$$g_{12} = V_{12}^{\rm eff} + V_{12}^{\rm eff}G_0 g_{12}, \quad (3)$$

for g_{12} with the nucleon propagator G_0 including the Pauli exclusion operator. Here the single-particle energy $e_{\boldsymbol{k}}$ for a nucleon with momentum $\boldsymbol{k}$ in the denominator of G_0 is obtained by [9]

$$e_{\boldsymbol{k}} = \langle \boldsymbol{k}|T|\boldsymbol{k}\rangle + {\rm Re}[\mathcal{U}(\boldsymbol{k})], \quad (4)$$

with the single-particle potential,

$$\mathcal{U}(\boldsymbol{k}) = \sum_{\boldsymbol{k}'}^{k_{\rm F}}\langle \boldsymbol{k}\boldsymbol{k}'|g_{12} + \frac{1}{6}V_{12(3)}(1 + G_0 g_{12})|\boldsymbol{k}\boldsymbol{k}'\rangle_A, \quad (5)$$

where T is a kinetic-energy operator of nucleon with the mass m and $\boldsymbol{k}$ is related to the incident energy $E_{\rm in}$ as $E_{\rm in} = (\hbar\boldsymbol{k})^2/(2m) + {\rm Re}[\mathcal{U}]$. When $E_{\rm in} > 0$, the single-particle potential is nothing but an optical potential of an extra nucleon in nuclear matter. Similar calculations, but in the second-order perturbation, of the optical potential in the framework of Ch-EFT was reported by Holt *et al.* [34]. The present formulation

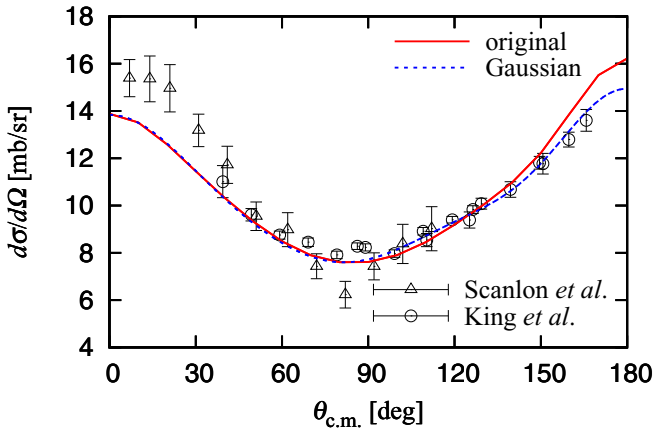

FIG. 1. (Color online) Differential cross sections for neutron-proton scattering at $E_{\rm in} \simeq 65$ MeV in free space. The solid (dashed) curves represent the results of the original (Gaussian) chiral t matrix. Experimental data are taken from Refs. [38,39].

is consistent with theirs by virtue of the factor 1/6 in Eq. (5) [9].

In the present BHF calculation, the cutoff energy $\Lambda = 550$ MeV is used with the form factor $\exp\{-(q'/\Lambda)^6 - (q/\Lambda)^6\}$ both for V_{12} and $V_{12(3)}$. The low-energy constants of chiral forces are taken from Ref. [35] as $(c_1,c_3,c_4) = (-0.81,-3.4,3.4)$ in units of GeV^{-1}, and the other constants $(c_D,c_E) = (-4.381,-1.126)$ are from Ref. [8]. Other sets of low-energy constants present in the literature [36] are expected to give essentially the same results. Furthermore, the variation of g matrices is much reduced in the effective 2NF level when 3NFs are incorporated consistently [9]. In addition, the net effect of c_D and c_E is small, when $c_D \simeq 4c_E$. This relation is well satisfied in various calculations for light nuclei in Ref. [37] and also for nuclear matter in Ref. [8] and the present work. As for $\mathcal{U}$, our results are similar to those of second-order perturbation calculations [34] for the real part, but for the imaginary part the former is more absorptive than the latter. This may be originated in the full ladder-summation in g-matrix calculations.

Figure 1 shows differential cross sections for neutron-proton scattering at $E_{\rm in} \simeq 65$ MeV in free space (in the limit of $\rho = 0$), where $E_{\rm in}$ stands for an incident energy in the laboratory system. The solid and dashed lines denote the results of original and Gaussian chiral t matrices, respectively; note that the g matrix is reduced to the t matrix in the limit of $\rho = 0$. Thus the Gaussian t matrix well reproduces the result of the original chiral t matrix.

The g matrix can be classified with $S,T,E_{\rm in}$, and $k_{\rm F}$ as $g^{ST}(k_{\rm F},E_{\rm in})$. Hence $\mathcal{U}$ can be decomposed into $\mathcal{U} = \sum_{ST}(2S+1)(2T+1)\mathcal{U}^{ST}$ with $\mathcal{U}^{ST}$ defined by Eq. (5) in which g and $V_{12(3)}$ are replaced by g^{ST} and $V_{12(3)}^{ST}$, respectively. Thus, $\mathcal{U}^{ST}$ means the single-particle potential in each spin-isospin channel.

Figure 2 shows $k_{\rm F}$ dependence of $\mathcal{U}^{ST}$. The squares and circles stand for the results of the original chiral g matrix with and without chiral 3NF, respectively. The difference between the two results mainly stems from the 2π-exchange diagram

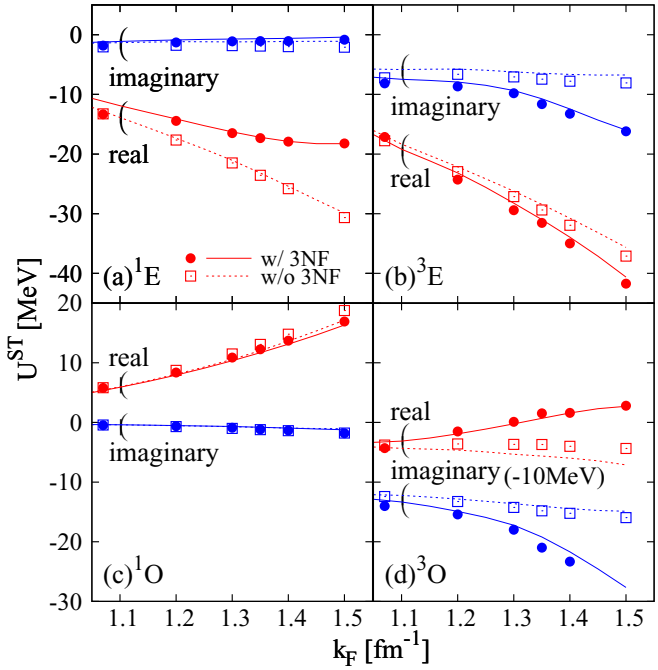

FIG. 2. (Color online) $k_{\rm F}$ dependence of $\mathcal{U}^{ST}$ at $E_{\rm in} = 65$ MeV for (a)^{1}E, (b) ^{3}E, (c) ^{1}O, and (d) ^{3}O. Squares (circles) mean the results of the original chiral g matrix with (without) 3NF. The solid (dashed) lines represent the results of the Gaussian chiral g matrix with (without) 3NF. For ^{3}O, the imaginary part is shifted down by 10 MeV.

in chiral 3NF. Particularly for nucleon and ^{4}He scattering, the region $k_{\rm F} \lesssim 1.35$ fm^{-1} ($\rho \lesssim \rho_0$) is important. For the spin-triplet channels (^{3}E and ^{3}O), the 2π-exchange 3NF enhances tensor correlations and makes transitions between different states stronger, and eventually it makes the imaginary part of $\mathcal{U}^{ST}$ more absorptive. For ^{1}E, chiral-3NF effects are large and repulsive, which corresponds to the suppression of Δ isobar excitations in nuclear medium in a conventional picture. The solid and dashed lines correspond to the results of the Gaussian chiral g matrix with and without chiral 3NF, respectively. The Gaussian chiral g matrix well reproduces the results of the original chiral g matrix. The potentials in the parity-odd channels, ^{1}O and ^{3}O, are small.

B. Folding model

The formulation of SF and DF models is summarized in Ref. [28], together with the relation between the two models. The folding potential is composed of the direct and knock-on exchange components. The latter component makes the potential nonlocal, but it can be localized with high accuracy by the Brieva-Rook (local momentum) approximation [15]. The reliability of this approximation is shown in Refs. [40,41]. The resultant folding potential $U(\boldsymbol{R})$ is a function of the relative coordinate $\boldsymbol{R}$ of projectile and target. The odd (^{3}O and ^{1}O) channels of g^{ST} are almost canceled between the direct and knock-on exchange components, and hence $U(\boldsymbol{R})$ is determined mainly by the even (^{3}E and ^{1}E) g matrices; e.g., see Refs. [24,25]. The S matrices for NA and ^{4}He elastic

scattering are obtained by solving a one-body Schrödinger equation with $U(\boldsymbol{R})$.

For ^{40}Ca, ^{58}Ni, and ^{208}Pb targets, the matter densities are calculated with the spherical Hartree-Fock (HF) method using the Gogny-D1S interaction [42]. The spurious center-of-mass (c.m.) motions are removed in a standard prescription [21]. For ^{4}He, we take phenomenological density determined from electron scattering [43] in which the finite-size effect of proton charge is unfolded by using a standard procedure [44].

III. RESULTS

First, we consider proton elastic scattering at $E_{\rm in} = 65$ MeV from ^{40}Ca, ^{58}Ni, and ^{208}Pb targets. In Fig. 3, differential cross sections $d\sigma/d\Omega$ and vector analyzing powers A_y are plotted as a function of scattering angle $\theta_{\rm c.m.}$ in the c.m. system. The solid and dashed lines stand for the results of the chiral g matrix with and without 3NF effects, respectively. Chiral-3NF effects are small at forward and middle angles where the experimental data [45] are available, because the scattering is governed by the potential in the surface region where 3NF effects are small because of low density. Only an exception is A_y at $\theta_{\rm c.m.} \simeq 60^\circ$ for ^{40}Ca and ^{58}Ni targets. Chiral-3NF effects enhance the spin-orbit part of $U(\boldsymbol{R})$ by a factor of about 30%, which may be the reason for this improvement. We confirmed that chiral-3NF effects are small also for $\sigma_{\rm R}$.

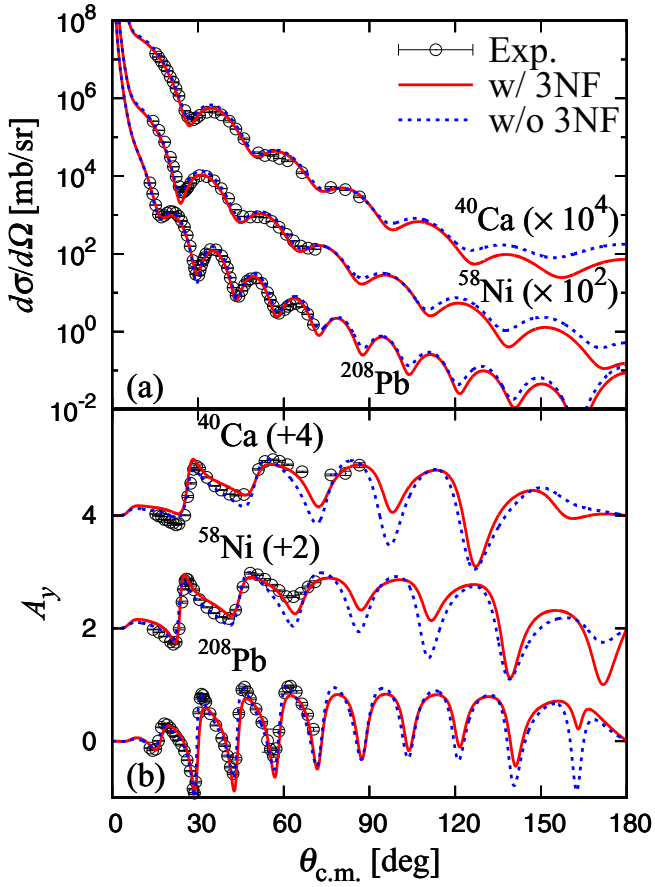

FIG. 3. (Color online) Angular distribution of (a) differential cross sections and (b) vector analyzing powers for proton elastic scattering at 65 MeV. The solid (dashed) lines denote the results of chiral g matrix with (without) 3NF effects. Each cross section is multiplied by the factor shown in the figure, while each vector analyzing power is shifted up by the number shown in the figure. Experimental data are taken from Ref. [45].

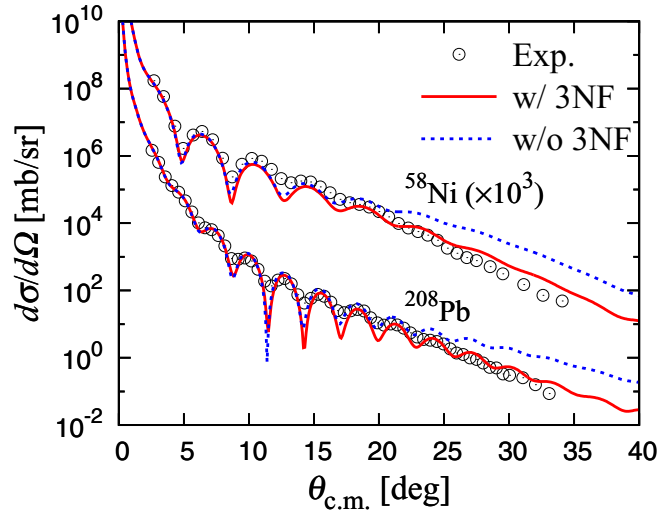

FIG. 4. (Color online) Angular distribution of differential cross sections for ^{4}He scattering at 72MeV/nucleon from ^{58}Ni and ^{208}Pb targets. The solid (dashed) lines denote the results of the chiral g matrix with (without) 3NF effects. Each cross section is multiplied by the factor shown in the figure. Experimental data are taken from Ref. [46].

Next, we show the angular distribution of $d\sigma/d\Omega$ for ^{4}He scattering at 72 MeV/nucleon from ^{58}Ni and ^{208}Pb targets in Fig. 4. The solid and dashed lines denote the results of the chiral g matrix with and without 3NF effects, respectively. For both targets, chiral-3NF effects are sizable at middle angles $\theta_{\rm c.m.} \gtrsim 20^\circ$ where the experimental data [46] are available.

The scattering amplitude can be decomposed into the near- and far-side components [47]. When a detector is set on the right-hand side of the target, the outgoing wave going through the right-hand (left-hand) side of the target is called the near-side (far-side) scattering. The near-side (far-side) component is mainly induced by repulsive Coulomb (attractive nuclear) force, and in general the near-side (far-side) component dominates forward-angle (middle-angle) scattering. For both ^{58}Ni and ^{208}Pb targets, large oscillations seen in the range $\theta_{\rm c.m.} = 5$–20° are a consequence of the interference between the near- and far-side components. When the scattering is dominated by the far-side component, $d\sigma/d\Omega$ has no oscillation and is sensitive to the change of nuclear force. The far-side dominance appears at $\theta_{\rm c.m.} > 20^\circ$. Chiral-3NF effects thus appear in the far-side dominant angles sensitive to the change of nuclear force.

Figure 5 shows the central part $U_{\rm CE}(R)$ of U for ^{4}He + ^{208}Pb scattering at 72MeV/nucleon. The solid and dashed lines correspond to the results of the chiral g matrix with and without 3NF effects, respectively. Chiral 3NF, mainly in its the 2π-exchange diagram, makes $U_{\rm CE}(R)$ less attractive

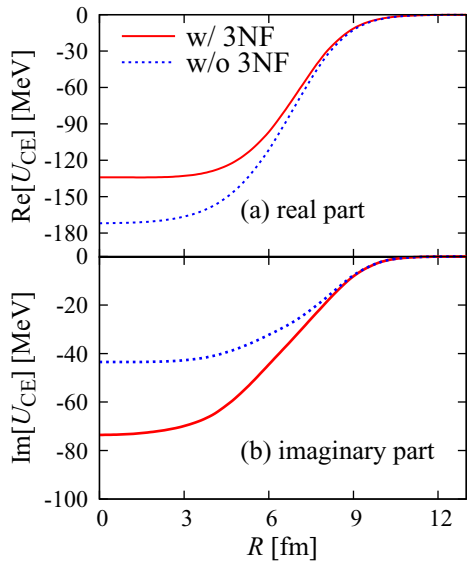

FIG. 5. (Color online) R dependence of the central part of the folding potential for ^{4}He + ^{208}Pb elastic scattering at $E =$ 72 MeV/nucleon. These (a) and (b) correspond to the real and imaginary parts of $U_{CE}(R)$, respectively. The solid (dashed) lines represent the results of chiral g matrix with (without) chiral 3NF.

and more absorptive. This repulsive effect of chiral 3NF in $U_{CE}(R)$ comes from the repulsion in the ^{1}E channel of g^{ST}. The repulsive nature suppresses $d\sigma/d\Omega$ at $\theta_{c.m.} > 20^\circ$ for ^{4}He scattering, whereas stronger absorption from chiral 3NF better separates the far-side amplitude from the near-side one.

IV. SUMMARY

We investigated the effects of chiral NNLO 3NF on proton scattering at 65 MeV and ^{4}He scattering at 72 MeV/nucleon from heavier targets, using the standard BHF method and the g-matrix folding model. We evaluated the g matrix from N^{3}LO 2NF plus NNLO 3NF for positive energy in nuclear matter. The same calculations for negative energies account well for the empirical saturation properties of symmetric nuclear matter. Chiral-3NF effects are mainly originated in the 2π-exchange diagram. The 3NF contribution in the ^{3}E channel enhances tensor correlations to make the optical potential more absorptive. In the ^{1}E channel, the 3NF effect yields a repulsion that may correspond to the Pauli suppression of isobar Δ excitation in the nuclear-matter medium in the conventional picture.

Following the Melbourne-group procedure [16,32,33], we provided the chiral g matrix with a three-range Gaussian form by making a χ^2 fitting to the on-shell and near-on-shell parts of the original numerical g matrix. This Gaussian form makes the folding procedure much easier. The g-matrix folding model with chiral 3NF reproduces the experimental data with no adjustable parameter for proton and ^{4}He scattering. We found that chiral-3NF effects are small for proton scattering but sizable for ^{4}He scattering at middle angles $\theta_{c.m.} \gtrsim 20^\circ$ where the experimental data are available. Chiral 3NF yields repulsive and absorptive corrections to $U_{CE}(R)$ for both proton and ^{4}He scattering. ^{4}He scattering is dominated by the far-side scattering amplitude at middle angles $\theta_{c.m.} \gtrsim 20^\circ$. The repulsive nature of chiral 3NF suppresses the far-side scattering amplitude, whereas the absorptive nature of chiral 3NF better separates the far-side scattering from the near-side one. Chiral 3NF thus becomes sizable in the far-side dominant angle range. Note that the repulsive nature comes from the ^{1}E channel, whereas the absorptive nature from the ^{3}E channel. Phenomenological 3NFs also make repulsive corrections to $U_{CE}(R)$ [17–19]. However, the origin of the repulsion is different. It is interesting if the mechanism of producing the repulsive contributions is clarified by analyzing scattering data.

ACKNOWLEDGMENTS

This work is supported in part by Grant-in-Aid for Scientific Research (No. 25400266 and No. 26400278) from Japan Society for Promotion of Science.

[1] H.-W. Hammer, A. Nogga, and A. Schwenk, Rev. Mod. Phys. **85**, 197 (2013).
[2] J. Fujita and H. Miyazawa, Prog. Theor. Phys. **17**, 360 (1957); **17**, 366 (1957).
[3] E. Epelbaum, H.-W. Hammer, and Ulf-G. Meißner, Rev. Mod. Phys. **81**, 1773 (2009).
[4] R. Machleidt and D. R. Entem, Phys. Rep. **503**, 1 (2011).
[5] N. Kalantar-Nayestanaki, E. Epelbaum, J. G. Messchendorp, and A. Nogga, Rep. Prog. Phys. **75**, 016301 (2012).
[6] J. D. Holt, J. Menéndez, J. Simonis, and A. Schwenk, Phys. Rev. C **90**, 024312 (2014).
[7] A. Ekström *et al.*, Phys. Rev. C **91**, 051301(R) (2015).
[8] K. Hebeler, S. K. Bogner, R. J. Furnstahl, A. Nogga, and A. Schwenk, Phys. Rev. C **83**, 031301(R) (2011).
[9] M. Kohno, Phys. Rev. C **88**, 064005 (2013).
[10] T. Krüger, I. Tews, K. Hebeler, and A. Schwenk, Phys. Rev. C **88**, 025802 (2013).
[11] C. Drischler, V. Somá, and A. Schwenk, Phys. Rev. C **89**, 025806 (2014).
[12] T. Krüger, K. Hebeler, and A. Schwenk, Phys. Lett. B **744**, 18 (2015).
[13] N. Kaiser, Eur. Phys. J. A **48**, 135 (2012).
[14] M. Yahiro, K. Ogata, T. Matsumoto, and K. Minomo, Prog. Theor. Exp. Phys. **2012**, 01A206 (2012).
[15] F. A. Brieva and J. R. Rook, Nucl. Phys. A **291**, 299 (1977); **291**, 317 (1977); **297**, 206 (1978).
[16] K. Amos, P. J. Dortmans, H. V. Von Geramb, S. Karataglidis, and J. Raynal, in *Advances in Nuclear Physics*, edited by J. W. Negele and E. Vogt (Plenum, New York, 2000), Vol. 25, p. 275.
[17] T. Furumoto, Y. Sakuragi, and Y. Yamamoto, Phys. Rev. C **78**, 044610 (2008).
[18] S. Rafi, M. Sharma, D. Pachouri, W. Haider, and Y. K. Gambhir, Phys. Rev. C **87**, 014003 (2013).

[19] Y. Yamamoto, T. Furumoto, N. Yasutake, and Th. A. Rijken, Phys. Rev. C **88**, 022801 (2013).
[20] B. Sinha, Phys. Rep. **20**, 1 (1975); B. Sinha and S. A. Moszkowski, Phys. Lett. B **81**, 289 (1979).
[21] T. Sumi *et al.*, Phys. Rev. C **85**, 064613 (2012).
[22] K. Egashira, K. Minomo, M. Toyokawa, T. Matsumoto, and M. Yahiro, Phys. Rev. C **89**, 064611 (2014).
[23] R. Machleidt, K. Holinde, and Ch. Elster, Phys. Rep. **149**, 1 (1987).
[24] M. Toyokawa, K. Minomo, M. Kohno, and M. Yahiro, J. Phys. G **42**, 025104 (2015).
[25] K. Minomo, M. Toyokawa, M. Kohno, and M. Yahiro, Phys. Rev. C **90**, 051601(R) (2014).
[26] T. Izumoto, S. Krewald, and A. Faessler, Nucl. Phys. A **341**, 319 (1980).
[27] M. Yahiro, K. Minomo, K. Ogata, and M. Kawai, Prog. Theor. Phys. **120**, 767 (2008).
[28] M. Toyokawa, T. Matsumoto, K. Minomo, and M. Yahiro, Phys. Rev. C **91**, 064610 (2015).
[29] S. Sasabe, T. Matsumoto, S. Tagami, N. Furutachi, K. Minomo, Y. R. Shimizu, and M. Yahiro, Phys. Rev. C **88**, 037602 (2013).
[30] T. Matsumoto and M. Yahiro, Phys. Rev. C **90**, 041602(R) (2014).
[31] S. Watanabe *et al.*, Phys. Rev. C **89**, 044610 (2014).
[32] H. V. von Geramb, K. Amos, L. Berge, S. Bräutigam, H. Kohlhoff, and A. Ingemarsson, Phys. Rev. C **44**, 73 (1991).
[33] P. J. Dortmans and K. Amos, Phys. Rev. C **49**, 1309 (1994).
[34] J. W. Holt, N. Kaiser, G. A. Miller, and W. Weise, Phys. Rev. C **88**, 024614 (2013).
[35] E. Epelbaum, W. Glöckle, and Ulf-G. Meißner, Nucl. Phys. A **747**, 362 (2005).
[36] D. R. Entem and R. Machleidt, Phys. Rev. C **68**, 041001 (2003).
[37] A. Nogga, P. Navrátil, B. R. Barrett, and J. P. Vary, Phys. Rev. C **73**, 064002 (2006).
[38] J. P. Scanlon, G. H. Stafford, J. J. Thresher, P. H. Bowen, and A. Langsford, Nucl. Phys. **41**, 401 (1963).
[39] N. S. P. King, J. D. Reber, J. L. Romero, D. H. Fitzgerald, J. L. Ullmann, T. S. Subramanian, and F. P. Brady, Phys. Rev. C **21**, 1185 (1980).
[40] K. Hagino, T. Takehi, and N. Takigawa, Phys. Rev. C **74**, 037601 (2006).
[41] K. Minomo, K. Ogata, M. Kohno, Y. R. Shimizu, and M. Yahiro, J. Phys. G **37**, 085011 (2010).
[42] J. F. Berger, M. Girod, and D. Gogny, Comput. Phys. Commun. **63**, 365 (1991).
[43] H. de Vries, C. W. de Jager, and C. de Vries, At. Data Nucl. Data Tables **36**, 495 (1987).
[44] R. P. Singhal, M. W. S. Macauley, and P. K. A. De Witt Huberts, Nucl. Instrum. Methods **148**, 113 (1978).
[45] H. Sakaguchi *et al.*, Phys. Lett. B **89**, 40 (1979); **99**, 92 (1981).
[46] B. Bonin *et al.*, Nucl. Phys. A **445**, 381 (1985).
[47] R. C. Fuller, Phys. Rev. C **12**, 1561 (1975).